Desalination and Water Treatment
www.deswater.com

doi:10.5004/dwt.2018.23024

132 (2018) 30–41
November

Hydrodynamic evaluation of retention time in non-steady state reactors using the *N-CSTR* model and numerical simulation

Daniel Jadyr L. Costa[a,*], Julio Cesar de S.I. Gonçalves[b], Marcius F. Giorgetti[c], Eduardo C. Pires[c]

[a]*Department of Environmental Sciences, Federal University of São Carlos, Rod. Washington Luís, km 235, 13565-905, São Carlos, SP, Brazil, email: danielcosta.geo@gmail.com (D.J.L. Costa)*
[b]*Department of Environmental Engineering, Federal University of Triângulo Mineiro, Av. DrRandolfo Borges Jr, 1250, Univerdecidade, 38064-200, Uberaba, MG, Brazil, email: sig.julio@gmail.com (J.C.S.I. Gonçalves)*
[c]*Department of Hydraulics and Sanitary Engineering, São Carlos School of Engineering, University of São Paulo, Av. Trabalhador Sãocarlense, 400, 13566-590, São Carlos, SP, Brazil, email: marciusg@sc.usp.br (M.F. Giorgetti), ecpires@sc.usp.br (E.C. Pires)*

Received 23 January 2018; Accepted 25 August 2018

ABSTRACT

There are many reactors that operate under non-steady state flow conditions, particularly in water supply and wastewater treatment systems. Knowledge concerning hydrodynamics of reactors is fundamental for their design and operation, however under non-steady state conditions, methods to evaluate hydrodynamic conditions use complex models and are difficult to apply on a daily basis. Consequently, when evaluating reactors, many engineers and technicians use conventional methods developed for steady-state conditions, which is a conceptual error that could lead to inconsistent results. To partially overcome this difficulty, a computational procedure established for hydrodynamic evaluation of reactors is presented in this paper under a non-steady flow, using the continuous stirred-tank reactor (*N-CSTR*) model. Moreover, the Vensim 6.3 software from Ventana Systems was used. After conducting experiments using the saline tracer, as well as calibrating and validating the model with experimental results, it was observed that the procedure is suitable for predicting the hydrodynamic behavior of reactors under non-steady state conditions with sinusoidal flow rate, for which it was tested.

Keywords: Hydrodynamic; Mathematical model; *N-CSTR* model; Non-steady state

1. Introduction

Biochemical and chemical reactor designs show an understanding of the hydraulic transport of materials and the biochemical and chemical reactions which take place within the reactor. The first component (hydraulic transport) defines the hydrodynamic behavior of the system and is characterized essentially by physical factors such as the geometry of the reactor, length, width and depth ratio, ways of distributing feeders, the flow velocity and the degree of mixing. The second component (biochemical and chemical reactions) is governed by the reaction kinetics, reagent concentration in the case of chemical reactions and by affinity between the substrate and biomass in the case of biochemical reactions. Meeting the objectives concerning the reactor design depends on the inter-relation between these components. The hydrodynamic variable could interfere significantly in the efficiency of the system as it has a direct influence on the performance of the reactions.

Hydrodynamic characterization is performed to identify the existing anomalies in reactor flows, as well as to provide data to verify if the flow is developing according to the design aspects of the reactor design. One of the main hydrodynamic aspects analyzed is the degree of mixing, which is intended to demonstrate if the flow pattern determines a complete mixing or plug flow regime [1]. This aspect can be

*Corresponding author.

characterized by parameters as the dispersion number (d), which is the inverse of the Péclet number ($d = P_{é}^{-1}$), and the continuous stirred-tank reactor (*N-CSTR*) model [2–5].

Hydrodynamic characterization procedures should be carried out during the normal operation of the reactors. There are reactors that operate under a non-steady state flow regime, in addition to those that undergo intermittent operations that include periods of starting and stopping operations due to maintenance and seasonality of the reactor's operation [6–9].

The mathematical model to be applied in the analysis must be compatible with the flow and operation of the reactor. This may cause some difficulties when handling the data for non-steady state flows, because for these conditions two transient and simultaneous situations must be characterized, which are: i) the conservative tracer mass transport, and ii) the transient behavior or non-steady state flow.

Thus, due to these difficulties, by and large, the application of a developed mathematical model considering the hypothesis of a steady state regime is conducted [10–12] for any situation, even if this implies incompatibility between the real situation and the mathematical model chosen. In this paper, the errors found in such situations were accounted for and the error reduction was also verified after applying a new mathematical model, which is compatible with the non-steady flow regime, and was developed according to the procedures presented here.

Based on injecting an inert tracer inside a reactor in operation, Danckwerts [10] showed a way of determining the hydraulic residence time distribution. Levenspiel [12] used a methodology to analyze the experimental results obtained from reactors which operate under steady state flow conditions. These methodologies are considered conventional and are often used to evaluate the hydrodynamic performance of reactors. However, they are not suitable for reactors that are operated under non-steady state flow conditions [6–9,13–17], and therefore there is a need to develop new procedures and models that are attractive and appropriate for these situations.

Some authors have made advances in terms of hydrodynamic flow analysis in reactors, which operate under non-steady state flow conditions[18–22]. As computer and data processors are continuously being developed, existing models can be improved or new models can be made with new interfaces, which use robust numerical models to solve differential equations found in these situations.

Considering the occurrence of the two transient and simultaneous situations that occur during the tracer tests (tracer plume transport and non-steady state flow regime), there is a development of a complex event from the physical and mathematical point of view and its modeling refers to a system of differential equations whereby its solution requires familiarization with numerical techniques and computational programming. Depending on the condition, a specialist in numerical methods may be required [23]. A more practical alternative is to use computational packages, called software tools that automatically integrate differential equations using calculation routines [23], such as Stella [24] (Isee systems, Inc., 2018), MATLAB/Simulink [25] (The MathWorks, Inc. 2018) and Vensim [26] (Ventana Systems, Inc. 2018) [27]. All these packages have a graphical user interface (GUI), which can construct and manipulate models more easily and faster, when compared to conventional programming, which requires directly developing algorithms.

Although all of these software tools are sufficiently effective in quantitative environmental modelling, selecting a particular software tool may depend on a number of factors [27]. The Vensim software was chosen due to the fact that the authors have expertise in this area, it has a user-friendly interface, it is free and it provides a simple way to construct models using stock and rate diagrams. The operating and construction mode of the models are essentially based on the principle of quantity conservation, including mass and energy. It is suitable software for dynamic systems that involve solving systems of linear and non-linear equations. Due to these characteristics, it has been used in a wide range of research areas, including transport and dispersion of pollutants in soil, water and air [28–31], the flow of macro-nutrients [32,33], hydrological simulations [34–36], and planning water supply sources [37–40].

This paper presents a computational procedure designed for hydrodynamic evaluation of reactors, which operate under non-steady state flow conditions, aiming to support water and wastewater treatment system analyses and forecasts.

2. Materials and methods

2.1. Theoretical background

Mathematical models for hydrodynamic evaluation of reactors can be developed by observing the response curve of the reactor after injecting a tracer. The response curve is an empirical representation of the tracer mass transport in the cross section of interest and the response is provided by the system due to the tracer dispersion phenomenon in the fluid medium. This type of dispersion can be considered as a composition between the lateral mixture (radial dispersion), where mainly the molecular and turbulent diffusions are active [41], and the longitudinal mixture (axial dispersion), which is caused mainly by the velocity gradient of the flow [42]. When a flow is represented by the continuous stirred-tank reactor (*N–CSTR*), it is assumed that the lateral mixing is fully developed, and the longitudinal mixing (D_L) becomes the main target to be characterized, so that its intensity is inversely proportional to the number of virtual reactors (N) in series, thus $DL \alpha N^{-1}$.

In various situations, longitudinal mixing is characterized by a single parameter, the "longitudinal dispersion coefficient", D_L, which has a surface area dimension per unit time [$L^2.T^{-1}$]. D_L can be influenced by quantities such as molecular diffusivity (D_m), the Péclet number ($P_é$), the Reynolds number (R_e) and the Schmidt number (S_c) [1,43–45]. D_L can be obtained using the advection-dispersion equation (ADE) [1,46], having the experimental data of the tracer mass concentration variation over time and space, and sampling in two sections of interest of the control volume, with subsequent adjustment of the equation to the experimental data, assuming D_L as the governing variable of the adjustment.

An alternative way of using the longitudinal dispersion coefficient is having knowledge about the E curve, as well as using the *N-CSTR* model. In this case, the tracer mass concentration needs to be obtained experimentally in the

reactor only over time and in only one section of interest. After injecting the pulse shape, the response curve or age distribution of tracer output, E curve [T^{-1}], can be obtained by the following relation [10,12]

$$E_{(t)} = \frac{C_{pulse(t)}}{MQ^{-1}} \tag{1}$$

where C_{pulse} is the tracer concentration during transport in the section of interest after pulse injection [$M{\cdot}L^{-3}$], M is the injected tracer mass [M], and Q is the flow rate [$L^3{\cdot}T^{-1}$].

Using mass balance, the tracer concentration (C) over time (t), in a continuous flow reactor and with complete mixing hypothesis, is obtained by the following relation

$$\left(\frac{dC}{dt}\right)_{one\ reactor} = -\frac{Q}{V}C' = -\frac{C'}{\bar{t}_t} \tag{2}$$

where V is the reactor volume [L^3], C' is the tracer concentration inside the reactor [$M{\cdot}L^{-3}$], $\bar{t}$ is the theoretical hydraulic retention time of the reactor [T].

The E curve distribution can be normalized so that the area under the curve is unity, therefore

$$\int_0^\infty E_{(t)}dt = 1 \tag{3}$$

The E curve normalized in the dimensionless time, $\left(\theta = \frac{t}{\bar{t}}\right)$ is called the E_θ curve, and it a dimensionless response curve, as follows

$$E_\theta = \bar{t}E \tag{4}$$

where $\bar{t}$ is the actual or experimental hydraulic retention time of the reactor. When the *N–CSTR* model is used, $\bar{t}$ consists of the multiplication between the number of virtual reactors in series (N) and the hydraulic retention time in each reactor. If all the virtual reactors had equal volumes, it follows that

$$\bar{t} = N\bar{t}_i \tag{5}$$

where $\bar{t}_i$ corresponds to the average hydraulic retention time in each virtual reactor inside the actual reactor. After C_{pulse} has been obtained experimentally, the response curve E_θ and the variable N, can be obtained using the following expression [11]

$$E_\theta = \left(N\bar{t}_i\right)E = N\frac{(N\theta)^{N-1}}{(N-1)!}\exp(-N\theta) \tag{6}$$

The determination of the number of virtual reactors in series (N), can be obtained using a least-squares fitting approach.

2.2. Flow regime and model development

The numerical simulations were performed using the Vensim 6.3 from Ventana Systems, Inc. [26]. The simulation model is based on using of the continuous stirred-tank reactor (*N-CSTR*) model for the flow behavior standard, where N is the number of reactors.

In this model, the simulations for mass transport are carried out considering the hypothesis of existence of axial dispersion and the absence of radial dispersion (fully developed) and viscous effects of the fluid. In order to study the non-steady state flow regime, a cyclic sinusoidal flow rate was applied, as defined by Eq. (7).

$$Q_{(t)} = \bar{Q} + Q_a \sin\left(\frac{2\pi}{T_p}t\right) \tag{7}$$

where $\bar{Q}$ is the mean flow rate [$L^3{\cdot}T^{-1}$], Q_a is the flow rate amplitude [$L^3{\cdot}T^{-1}$], t is an instant of time [T] and T_p is the oscillation period [T].

Considering a non-steady state flow regime with the flow velocity towards x varying according to Eq. (7) and the cross section area (A_c) of the reactor being uniform, for a fluid that flows in and out of the first reactor N_1, the concentration (C) is C_1, instantaneously reached after the tracer is injected, as it is an ideal stirred tank reactor. After the instantaneous tracer pulse its mass balance becomes

$$\left(\frac{dC}{dt}\right)_{reactor1} = \frac{dC_1}{dt} = -\frac{\bar{Q} + Q_a \sin\left(\frac{2\pi}{T_p}t\right)}{V}C_1 \tag{8}$$

where V is the volume of the reactor [L^3].

For the second reactor, the mass balance results in

$$\left(\frac{dC}{dt}\right)_{reactor2} = \frac{dC_2}{dt} = \frac{\bar{Q} + Q_a \sin\left(\frac{2\pi}{T_p}t\right)}{V}C_1 - \frac{\bar{Q} + Q_a \sin\left(\frac{2\pi}{T_p}t\right)}{V}C_2 \tag{9}$$

The general equation of the mass balance for each one of the following n reactors is

$$\left(\frac{dC}{dt}\right)_{reactor\ n} = \frac{dC_n}{dt} = \frac{\bar{Q} + Q_a \sin\left(\frac{2\pi}{T_p}t\right)}{V}C_{n-1} - \frac{\bar{Q} + Q_a \sin\left(\frac{2\pi}{T_p}t\right)}{V}C_n \tag{10}$$

To solve the problem, Eqs. (8)–(10) should be solved together, forming a system of differential equations as follows

$$\left(\frac{dC}{dt}\right)_{reactor1} = f_1(C_1, C_2, \ldots, C_n) \tag{11}$$

$$\left(\frac{dC}{dt}\right)_{reactor2} = f_2(C_1, C_2, \ldots, C_n) \tag{12}$$

$$\left(\frac{dC}{dt}\right)_{reactor\ n} = f_n(C_1, C_2, \ldots, C_n) \tag{13}$$

The solution of this system of equations requires the initial conditions of concentration (C_1) to be known. As practical restrictions prevent the experiment from corresponding exactly to the theoretical model, the value of C_1 was obtained from the model calibration step. The solution of this system of equations can be obtained by using numerical integration methods. The Vensim 6.3 software offers two numerical integration techniques: the Euler (RK1) method and the Runge-Kutta method of the 4th order (RK4). The RK4 presents a relative percentage error which is significantly less

than that presented by RK1 [47], therefore it was chosen to solve the differential equations used in this study.

The Vensim 6.3 provides a simple way to construct models using stock and rate diagrams. The operating and construction mode of the models were essentially based on the principle of mass conservation from a macroscopic point of view or control volumes.

In Fig. 1, a schematic representation can be seen of a stock and rate diagram showing the input and output rate of mass for a sodium chloride tracer (NaCl). The stocks are represented by rectangles and the input and output rates are represented by arrows that show the flow direction. The valves control the input and output rates. The stocks are also called integrals, while the rates are the derivatives.

Two platforms were created using an arrangement of stirred tank reactors in series, each represented by a rectangle. The first platform, called Platform 1, was created for simulations with a number of continuous stirred-tank reactors under a steady-state flow regime (*N-CSTR SS*) and the second platform, Platform 2, was created for simulations with a number of continuous stirred-tank reactors under a non-steady state flow regime and with the possibility of *by pass* flow (*N-CSTR NSS-b*), as can be seen in Figs. 2 and 3.

In Figs. 2 and 3, *N* refers to the last reactor of the simulation. In the software all the stirred tank reactors must be created to simulate the flow. In the simulations used with Platform 2, a 10% fraction of the inflow reactor for the *by pass* was adopted.

2.3. Experimental apparatus

The experiments were carried out using three polyvinyl chloride (PVC) tubular reactors positioned horizontally with the following dimensions: internal diameter (∅) of 4.8 cm, longitudinal length of 48 cm, which results in closed-closed conditions in a flow pattern at the boundaries. Reactor 1 was not packed and its working volume (volume occupied by the flow fluid) resulted in 869 mL; reactor 2 was packed with glass beads (silicon carbide) of an average diameter (∅) of 4.4 mm (large glass beads) and resulted in a working volume of 290 mL. Finally, reactor 3 was packed with glass beads having an average diameter (∅) of 2.4 mm (small glass beads), reaching a working volume of 255 mL. A Grundfos dosing pump (DDA 7.5 $L \cdot h^{-1}$) was used coupled to a programmable sinusoidal signal generator for flow rate variation. The reactors were fed with distilled water and sodium chloride (NaCl) was used as a tracer. The tracer was injected as an instantaneous pulse. The data was collected using a portable conductivity meter, with a resolution of up to 0.05 mg. L^{-1} of total dissolved solids (TDS). A diagram of the experimental apparatus is shown in Fig. 4.

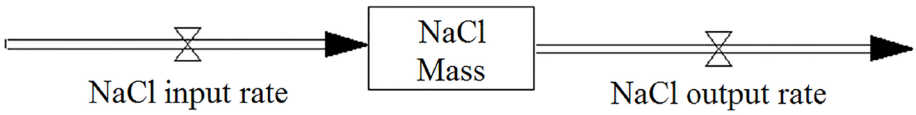

Fig. 1. Schematic representation of a stock and rate diagram showing the input and output for the NaCl tracer as used by Vensim 6.3.

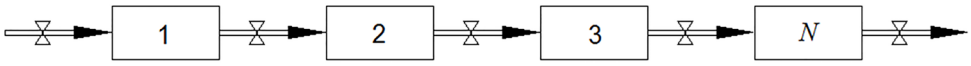

Fig. 2. Platform 1: Steady state flow and *N* continuous stirred-tank reactors (*N-CSTR SS* model).

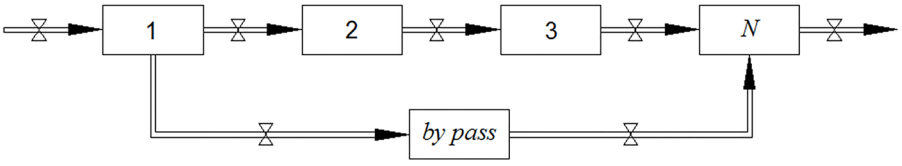

Fig. 3. Platform 2: Non-steady state flow with *by pass* and *N* continuous stirred-tank reactors (*N-CSTR NSS-b* model).

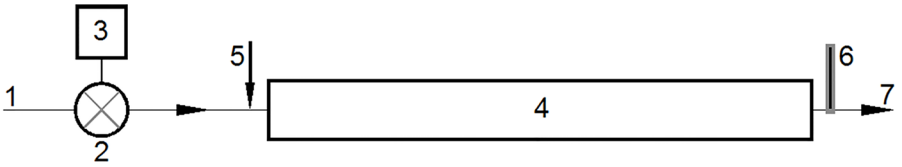

Fig. 4. Experimental apparatus. 1: inflow; 2: hydraulic pump; 3: programmable logic controller; 4: reactors (one reactor not packed, and two reactors packed); 5: tracer pulse; 6: conductivity meter; and 7: outflow.

As the aim of this research was to carry out an evaluation of the response curve (E_θ) of the reactor after injecting the tracer. The experiments were conducted in an abiotic, not reactive environment, resulting in an evaluation which was purely hydrodynamic.

The non-steady state regime with cyclic sinusoidal oscillation of flow rate adopted in this work is an idealized approximation of the typical hydrograph of wastewater treatment systems [48]. Table 1 shows a summary of the experimental conditions.

2.4. Experimental design

The hydrodynamic evaluations were carried out under steady-state and non-steady state flow regimes. The model was calibrated under a steady state regime and was validated under a non-steady state regime.

The calibration step defined the number N of continuous stirred-tank reactors obtained from the experimental results. After obtaining N, numerical simulations were performed in non-steady state flow regime, and therefore these numerical results were compared with the results from the real data and for the same experimental conditions. This last step was the validation.

The hydraulic conditions were as follows: mean hydraulic retention time ($\bar{t}$) of 10, 20 and 40 min; steady-state flow regime; and non-steady state flow regime. The steady-state flow regime was applied to two amplitude values, which were: i) 80% of flow rate variation in relation to the mean flow rate (Q_a = 0.8) and ii) 40% of flow rate variation in relation to the mean flow rate (Q_a = 0.4). In total, 52 experiments were carried out.

It was not possible to perform any experiments in reactor 1 under a non-steady state flow regime using a cyclic sinusoidal variation of 80% (Q_a = 0.8) and $\bar{t}$ = 10 min, as it would be necessary to reach a flow rate above the maximum capacity of the hydraulic pump that was used.

3. Results and discussion

Considering the 52 experiments carried out, in this paper some of the experimental results will be presented only through the E_θ curves. All results can be fully observed in Costa [49].

3.1. E_θ curves under a non-steady and steady-state regime

The graphs showing the results present the E_θ curve together with the dimensionless flow rate (Q_θ). The dimensionless flow rate refers to the real flow rate divided by the mean flow rate ($\bar{Q}$). For the flows under a steady-state regime, the dimensionless flow rate is equal to 1. For the flows under a non-steady state regime, the dimensionless flow rate oscillates in a cyclic sinusoidal way around value 1. The flow rate oscillation is defined by amplitude (Q_a) and its period (T_p), which was established as being equal to the mean hydraulic retention time of experiment ($\bar{t}$). The dimensionless time values are presented on the x-axis, which refers to the real time divided by the mean hydraulic retention time.

The E_θ curves obtained from the experiments carried out in the reactors packed with glass beads (reactors 2 and 3) show a different behavior from reactor 1. In Fig. 5, the E_θ curves obtained from experiments 1, 18, 24 and 36, respectively are presented, which were carried out under a steady-state. It can be observed that except for the initial concentration of the tracer shown by a circle in Figs. 5b, c and d (experiments 18, 24 and 32, respectively), there is a symmetry of the curves in the regions that precede and follow θ = 1. This shows that in these cases throughout the flow, the spread of the tracer in relation to its mass center took place more uniformly, and the dominant spreading mechanism is the advection with dispersion [50]. This is a typical behavior of plug flow reactors which usually have a relatively high Péclet number ($P_é$) [51].

On the contrary, in the E_θ curve in Fig. 5a (experiment 1), it can be observed that a significant amount of the tracer is detected relatively quickly in the output of the reactor followed by a slow drop in its concentration over time. In this case, the spreading tracer in relation to its mass center took place less uniformly, and the dominant spreading mechanism is the diffusion [50]. This is typical behavior of stirred tank flows, which have a relatively low Péclet number ($P_é$) [51].

The main feature that defined the dominant spreading mechanism of tracer was the packed media. The packing media with glass beads (in experiments 18, 24 and 32) creates a typical porous media, whereby in these conditions the advection with dispersion dominates the solute spreading, unless the flow velocity is slow or zero [50].

The circles presented in Figs. 5b, c and d, highlight in the E_θ curve the region in which a part of the tracer travels along the reactors at a velocity higher than the average. This effect is important from the phenomenological point of view of mass transference in reactors with this geometric arrangement and this type of packing media, as it shows the formation of preferential paths, which result in the partial anticipation of tracer output from the reactor. As the glass beads have a spherical shape when they are inside the reac-

Table 1
Summary of the experimental conditions

Reactor	Packing media	Working volume (mL)	Flow rate conditions	Hydraulic retention time (min)
1	None	869	1. Steady-state and	10, 20 and 30
2	Glass beads ∅ 4.4 mm	290	2. Non-steady state: varying sinusoidal with 0.4 $\bar{Q}$ and 0.8 $\bar{Q}$ amplitudes	
3	Glass beads ∅ 2.4 mm	255		

Note: all reactors had a length of 48 cm and an internal diameter (∅) of 4.8 cm.

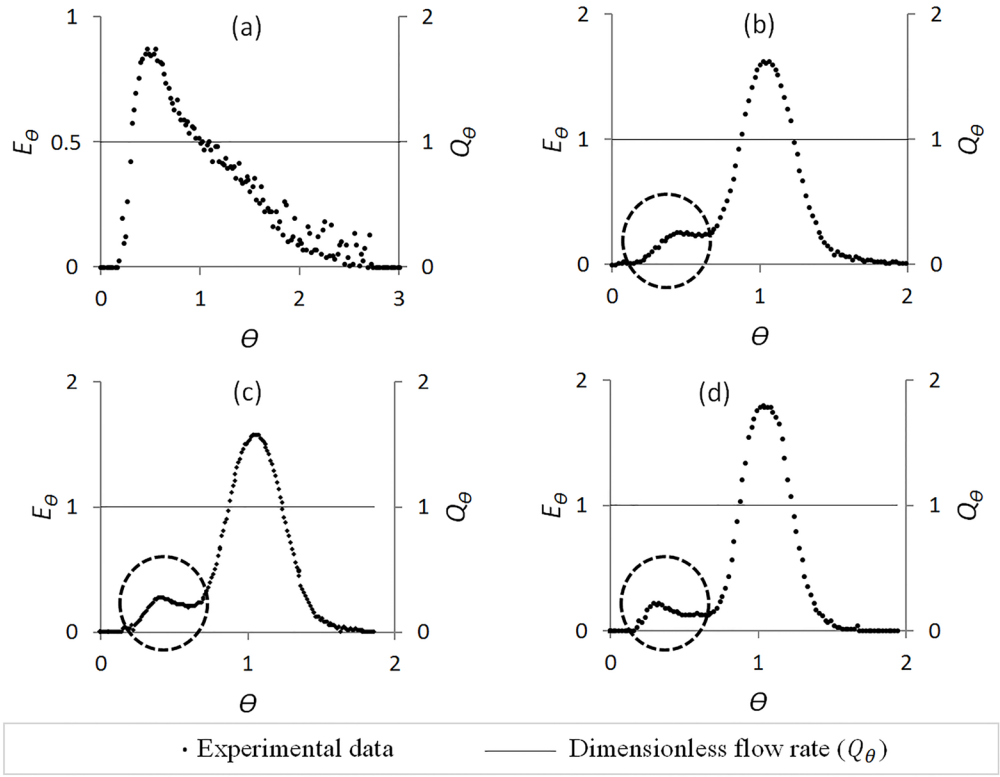

Fig. 5. E_θ curves for the experiments: (a) Experiment 1, carried out in reactor 1, $\bar{t}$ = 10 min, Q_a = 0; (b) Experiment 18, carried out in reactor 2, = 10 min, Q_a = 0; (c) Experiment 24, carried out in reactor 2, $\bar{t}$ = 20 min, Q_a = 0; and (d) Experiment 36, carried out in reactor 3, $\bar{t}$ = 10 min, Q_a = 0.

tor, they form interstices through which the fluid flows, so that on adjacent sides of the reactor´s walls these spaces are larger than those in other regions. This arrangement of the glass beads forms a peripheral area, which has more porosity or voids, as can be seen in Figs. 6a and c. A theoretical model of the velocity field is shown in Fig. 6b.

The heterogeneity of porosity in the cross section area of the reactor, characterized by an increased quantity of voids adjacent to the wall, causes a change in the flow known as the wall effect, which in some cases results in a *by pass flow* [52,53]. As the flow velocity is proportional to the porosity, the wall effect is responsible for the preferential flow close to the reactor boundary.

In Fig. 7, the E_θ curves presented were obtained from experiments 8, 15, 21 and 38, respectively, which were carried out under a non-steady flow rate. The behavior of the dimension less flow under a non-steady regime is presented with these figures. It can be observed that there is a significant difference in the behavior of the tracer out put in experiments 8 and 15 in relation to experiments 21 and 38, which is caused by the difference between the packing media of these reactors. It can be noted that in experiments 8 and 15 (Figs. 7a and b, respectively) that several peaks on the saline tracer concentrations appear. This takes place because the dominant spreading mechanism of the tracer is the diffusion while performing these experiments and 2-*CSTR* are found for both.

In experiments 21 and 38, carried out in reactors 2 and 3, respectively, the same effect of part of the advancing bulk flow shown in experiments 18, 24 and 36 (Figs. 5b, c and d) can be observed (Figs. 7c and d), demonstrating that in these cases preferential paths occurred. For experimental conditions of this work, under a non-steady state regime, it can be observed that the flow through a porous media (Figs. 7c and d) benefits from obtaining a less oscillatory curve when compared to the conditions without a packed media (Figs. 7a and b). The five tracer concentration peaks, shown in Figs. 7a and b, occurred because the longitudinal dispersion was quite intense inside the reactor, and therefore low *N-CSTR* values should be found (typical condition of stirred tank reactors). The opposite is also true, so that in Figs. 7c and d, only one tracer peak occurred, indicating that the presence of the porous medium inhibited the longitudinal scattering of the tracer, resulting in high *N-CSTR* values (typical condition of plug flow reactors).

3.2. Model calibration

For model calibration, the E_θ curves obtained from the experiments carried out under a steady-state flow rate in reactors 1, 2 and 3 were used. In Fig. 8, the models adjusted to the conditions of experiments 1, 18, 24 and 36, respectively, are presented.

It can be observed that for the experiments carried out in the packed reactors (experiments 18, 24 and 36), the resulting coefficient of determination (r^2) was less than that obtained from the experiment conducted in the unpacked

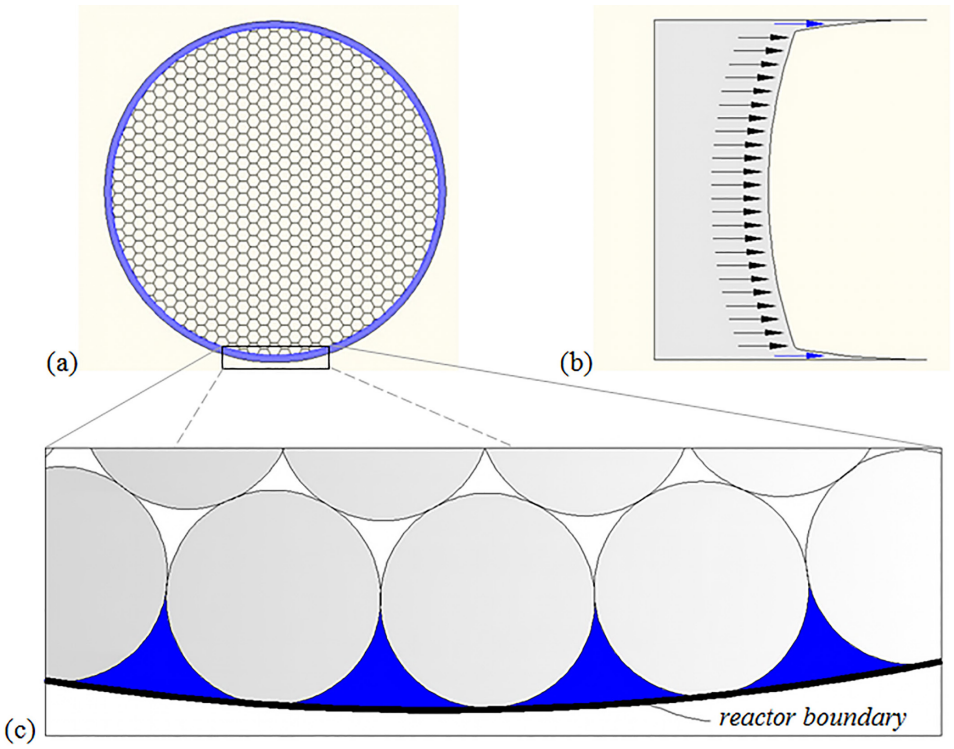

Fig. 6. (a) Cross section of the reactor showing the peripheral area with more porosity in blue; (b) Longitudinal cross section of there actor showing a theoretical model of the velocity field where there is a formation of preferential paths to the fluid; and (c) Peripheral area of the reactor enlarged.

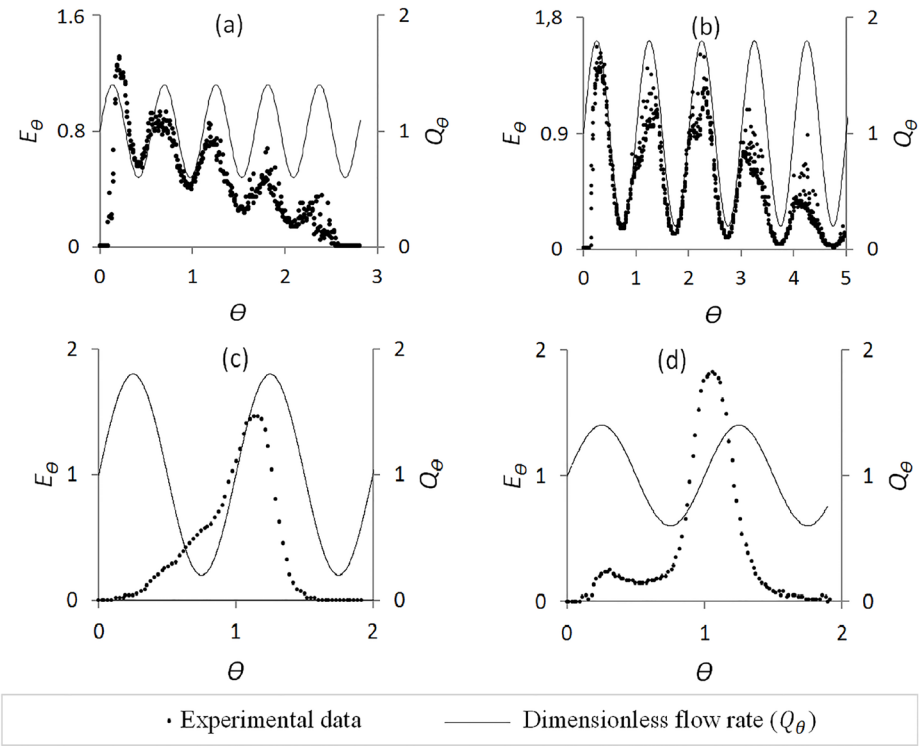

Fig. 7. E_θ curves for the experiments: (a) Experiment 8, carried out in reactor 1, $\bar{t}$ =20 min, Q_a = 0.4; (b) Experiment 15 carried out in reactor 1, $\bar{t}$ =40 min, Q_a = 0.8; (c) Experiment 21 carried out in reactor 2, $\bar{t}$ = 10 min, Q_a = 0.8; e (d) Experiment 38 carried out in reactor 3, $\bar{t}$ = 10 min, Q_a = 0.4.

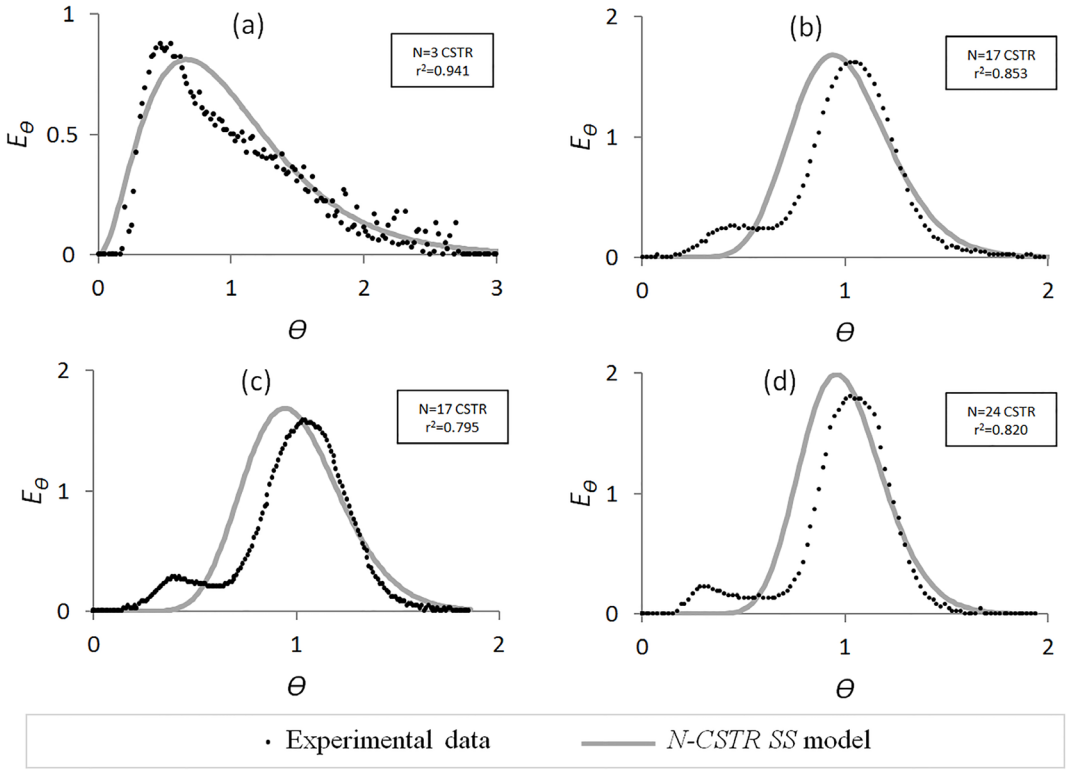

Fig. 8. E_θ curves with models in steady-state regime adjusted to the experiments: (a) Experiment 1, carried out in reactor 1, $\bar{t}$ = 10 min, Q_a = 0; (b) Experiment 18, carried out in reactor 2, $\bar{t}$ = 10 min, Q_a = 0; (c) Experiment 24, carried out in reactor 2, $\bar{t}$ = 20 min, Q_a = 0; and (d) Experiment 36, carried out in reactor 3, $\bar{t}$ = 10 min, Q_a = 0.

reactor (experiment 1). This is due to a limitation of the *N-CSTR SS* model. This model is not capable of considering the preferential flows (*by pass*) which take place in the near-wall region of the reactor, as it considers a complete mixing and a profile of uniform velocities in the sections, and consequently does not take into account the existence of the wall effect established in experiments 18, 24 and 36.

3.3. Model validation

Some experimental results to validate the model and confirm its predictions are presented in Fig. 9. Verification of the model´s predictive response in relation to the experimental data was obtained using the coefficient of determination (r^2), which in this case represents the capacity of the model to explain the hydrodynamic behavior of the flow based on the continuous stirred-tank reactor.

It can be observed in experiments 8, 15, 21 and 38 that the model was able to predict the behavior of the flows with a r^2 equal to 0.769, 0.859, 0.915 and 0.903, respectively.

Although there was a relatively poor fit in experiments 8 and 15 (Figs. 9a and b, respectively), r^2 equal to 0.769 and 0.859, the *N-CSTR NSS-b* model was able to represent the cyclic sinusoidal flow rate very well, and to some extent proportionately.

Having implemented the by-pass in the *N-CSTR NSS-b* model, it was possible to obtain a good fit to the experimental data, especially considering the occurrence of the partial preceding of tracer mass in the output of the reactor (preferential paths), as observed in experiments 21 and 38 (Figs. 9c and d, respectively), with r^2 equal to 0.915 and 0.903, respectively.

3.4. Comparison between the N-CSTR SS and N-CSTR NSS-b models

In Fig. 10, graphs that compare the *N-CSTR SS* and *N-CSTR NSS-b* models for experiments 8, 15, 21 and 38, respectively, are presented.

Considering the coefficients of determination (r^2), obtained for the *N-CSTR SS* and *N-CSTR NSS-b* models, it can be observed that using the *N-CSTR NSS-b* model resulted in better coefficient values. There has been an improvement in r^2 of approximately 104.5% for experiment 8; 120.3% for experiment 15; 32.0% for experiment 21 and 33.6% for experiment 38.

Improvements made to the fit for the experimental data, when using the *N-CSTR NSS-b* model, are due to the fact that for the development of this model two important mechanisms were considered for the studied flows, which are: i) a non-steady state flow rate with cyclic sinusoidal oscillation, and ii) the *by pass flow* that can simulate the wall effect caused by the boundary reactor in the flow.

Considering a total of 52 experiments, 26 were performed with Q_a = 0.4 and 24 were performed with Q_a = 0.8. The use of the *N-CSTR SS* model for these experiments resulted in an average coefficient of determination ($r^2_{average}$) of 0.674 and 0.578, for Q_a = 0.4 and Q_a = 0.8, respectively.

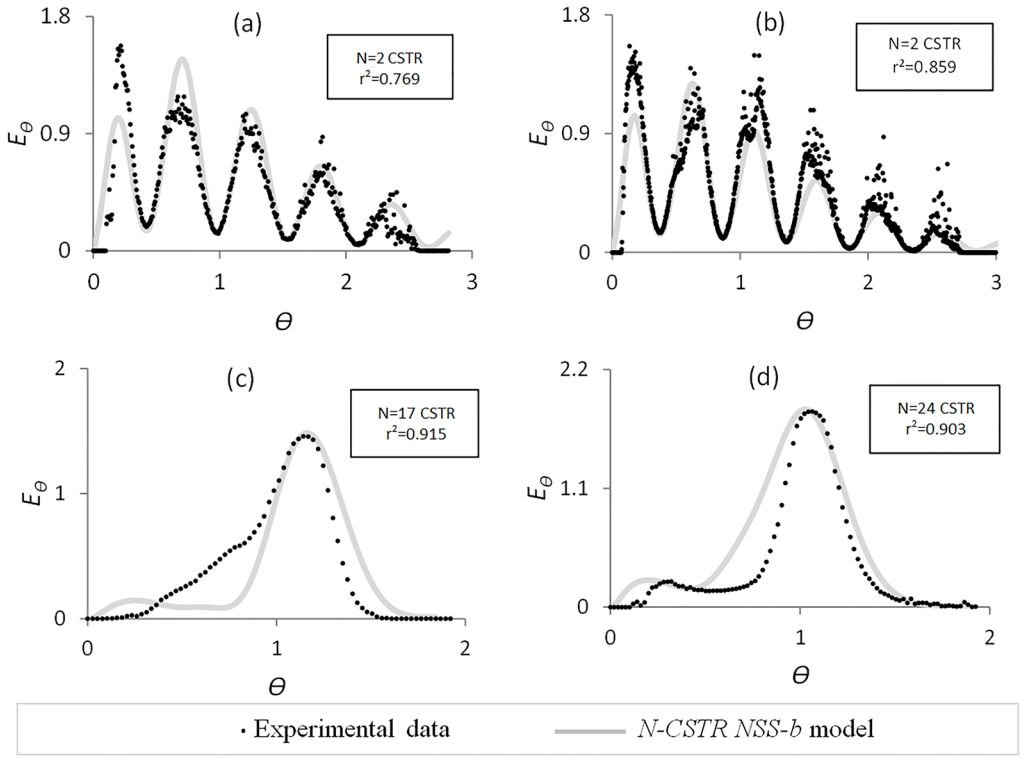

Fig. 9. E_θ curves with models under a non-steady regime adjusted to the experiments: (a) Experiment 8, carried out in reactor 1, $\bar{t}$ = 20 min, Q_a = 0.4; (b) Experiment 15 carried out in reactor 1, $\bar{t}$ = 40 min, Q_a = 0.8; (c) Experiment 21 carried out in reactor 2, $\bar{t}$ = 10 min, Q_a = 0.8; and (d) Experiment 38 carried out in reactor 3, $\bar{t}$ = 10 min, Q_a = 0.4.

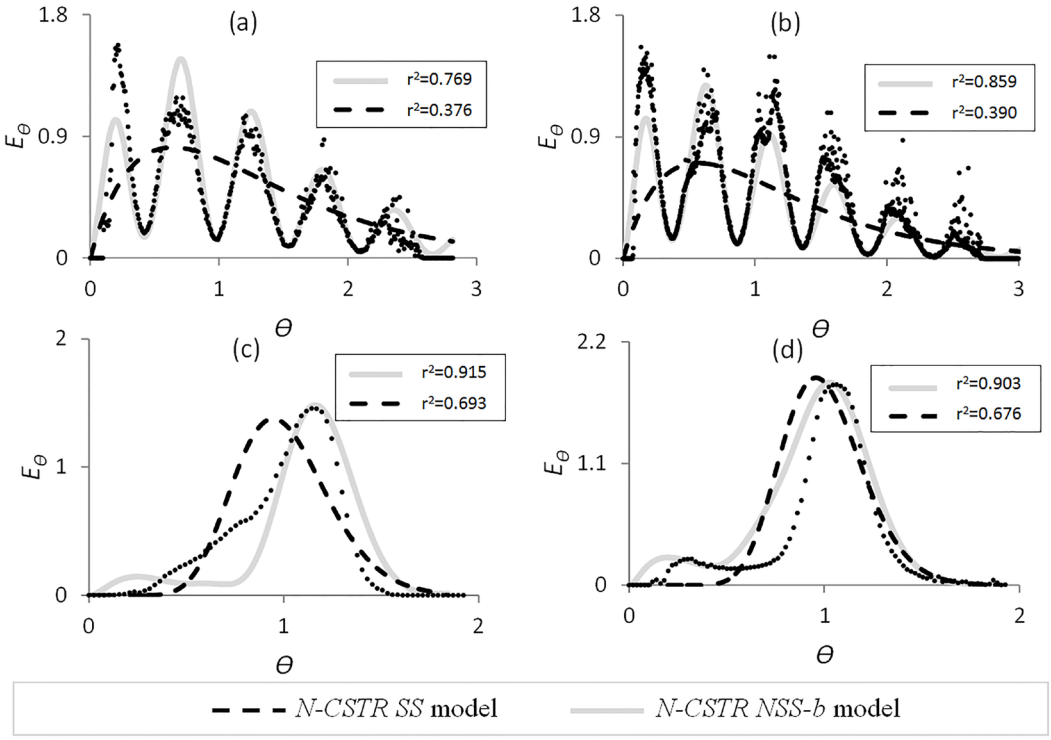

Fig. 10. Graphs comparing the *N-CSTR SS* model (dashed line) with the *N-CSTR NSS-b* model (continuous line) for the experiments: (a) Experiment 8, carried out in reactor 1, $\bar{t}$ = 20 min, Q_a = 0.4; (b) Experiment 15 carried out in reactor 1, $\bar{t}$ = 40 min, Q_a = 0.8; (c) Experiment 21 carried out in reactor 2, $\bar{t}$ = 10 min, Q_a = 0.8; e (d) Experiment 38 carried out in reactor 3, $\bar{t}$ = 10 min, Q_a = 0.4.

Table 2
Average coefficient determination and fitting improvement in the data

Model	($r^2_{average}$)	
	Q_a = 0.4	Q_a = 0.8
N-CSTR SS	0.674	0.578
N-CSTR NSS-b	0.842	0.845
Fitting improvement (%)	24.9	46.2

When using the *N-CSTR NSS-b* model, the $r^2_{average}$ obtained were 0.842 and 0.845, for Q_a = 0.4 and Q_a = 0.8, respectively. These data are presented in Table 2 whereby, in general, the highest differences in the fitting took place for the experiments with more amplitude of the flow rate, Q_a = 0.8. When comparing *N-CSTR SS* and *N-CSTR NSS-b* models, the latter caused a fitting improvement of 24.9% when Q_a = 0.4, and 46.2% when Q_a = 0.8. Therefore, the larger the flow rate amplitude, the better results are obtained using the *N-CSTR NSS-b* model.

Considering that the coefficient of determination (r^2) should be interpreted as the proportion of total variation of the dependent variable (E_θ), which is explained by the variation of the independent variable (θ), it is understood that the *N-CSTR NSS-b* model is able to explain, on average, 84.2% of the behavior of flows studied in this paper with Q_a = 0.4, and 84.5% of the flows with Q_a = 0.8.

The deviations were determined between the values estimated by the model and the values measured by the Standard Error (*SE*), using Eq. (14)

$$SE = \sqrt{\frac{1}{n}\sum_{i=1}^{n}\left(E_{\theta e} - E_{\theta m}\right)_i^2} \quad (14)$$

where n is the number of measures; $E_{\theta e}$ and $E_{\theta m}$ are respectively the estimated and measured values of the dimensionless exit tracer.

The Standard Error (*SE*) values for all the experiments carried out with Q_a = 0.4 are presented in Fig. 11.

For Q_a = 0.4, the main improvement in relation to *SE* occurred in reactor 2 when $\bar{t}$ = 40 min ($\bar{t}_3$). For this condition the *SE* with the *N-CSTR SS* model was 0.849 and the *SE* with the *N-CSTR NSS-b* model was 0.166, representing a reduction in *SE* value of 80.4%. The condition in which there was the least change was in reactor 1 when $\bar{t}$ = 10 min ($\bar{t}_1$). In this case, the *SE* with the *N-CSTR SS* model was 0.209 and the *SE* with the *N-CSTR NSS-b* model was 0.201, which shows a reduction in the *SE* value of only 3.8%. Considering all the experiments carried out with Q_a = 0.4, on average the *SE* with the *N-CSTR SS* model was 0.416 and the *SE* with the *N-CSTR NSS-b* model was 0.238, resulting in an average reduction in the *SE* value of 42.7%.

The Standard Error (*SE*) values for all the experiments carried out with Q_a = 0.8, are presented in Fig. 12.

For Q_a = 0.8, the mainly improvement in relation to *SE* also occurred in reactor 2 when $\bar{t}$ = 40 min ($\bar{t}_3$). For this condition, the *SE* with the *N-CSTR SS* model was 0.580 and the *SE* with the *N-CSTR NSS-b* model was 0.234, resulting in a reduction in the *SE* value of 59.7%. The condition in which there was a least change was in reactor 1 when $\bar{t}$ = 20 min ($\bar{t}_2$). In this case the *SE* with the *N-CSTR SS* model

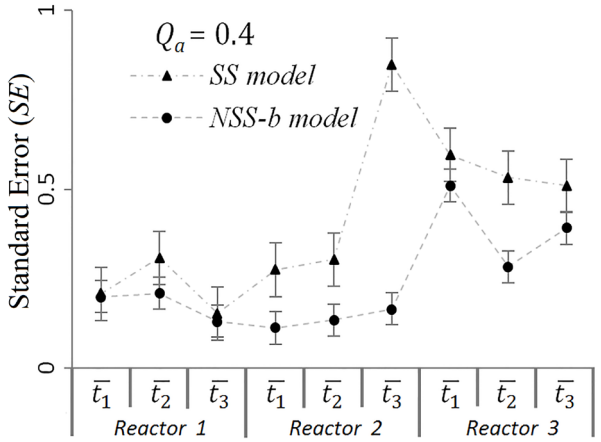

Fig. 11. Standard Error (*SE*) with Q_a = 0.4. Hydraulic retention times: $\bar{t}_1$ =10 min; $\bar{t}_2$ =20 min; $\bar{t}_3$ =40 min.

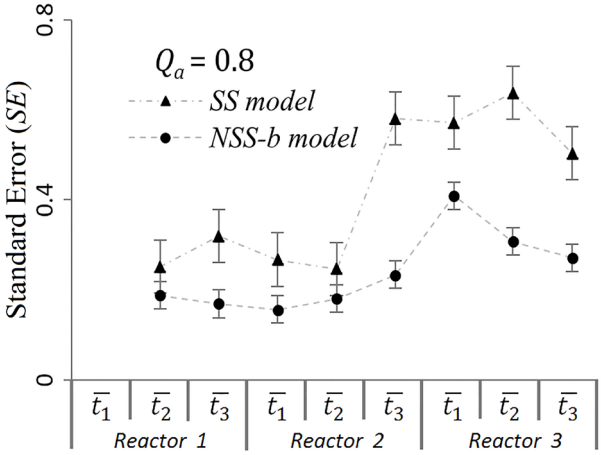

Fig. 12. Standard Error (*SE*) with Q_a = 0.8. Hydraulic retention times: $\bar{t}_1$ =10 min; $\bar{t}_2$ =20 min; $\bar{t}_3$ =40 min.

was 0.251 and the *SE* with the *N-CSTR NSS-b* model was 0.188. The reduction in the *SE* value was 25.3%. Considering all the experiments carried out with Q_a = 0.8, on average the *SE* with the *N-CSTR SS* model was 0.422 and the *SE* with the *N-CSTR NSS-b* model was 0.239, which represents an average reduction in the *SE* value of 43.3%.

4. Conclusions

Based on the results, it can be observed that the *N-CSTR NSS-b* model can be suitable to evaluate the hydrodynamic behavior of reactors in conditions under a non-steady state flow regime and which are packed by media capable of forming preferential paths in the flow. The model can be useful for designing and operating reactors. However, as any other model, its application should be limited to the conditions in which it was developed. The flows and simulations were carried out on a laboratory scale in an abiotic environment and the flow rate variation in a cyclical sinusoidal variation.

Considering the spatial dimensions, the developed model was conceptually one-dimensional, thus depending on the type of analysis required it is likely that for some full-scale reactors, its application will not be as successful due to the three-dimensional character of the flow gaining importance. Full-scale applications could require the need to use two or three-dimensional models which consider the gradient of momentum and mass transfer throughout the cross and longitudinal sections of the reactors.

Acknowledgements

The authors would like to thank the National Council for Scientific and Technological Development (CNPq) for the doctorate scholarship awarded to the first author and the Research Productivity Grant given to Prof. Eduardo Cleto Pires.

Symbols

A_c [L^2]	—	Cross section area
ADE	—	Advection-dispersion equation
D_L [$L^2 \cdot T^{-1}$]	—	Longitudinal dispersion coefficient
D_m [$L^2 \cdot T^{-1}$]	—	Molecular diffusion
E_θ [-]	—	Dimensionless exit curve
N-CSTR [-]	—	Number of continuous stirred-tank reactors
Q [$L^3 \cdot T^{-1}$]	—	Flow rate
$\bar{Q}$ [$L^3 \cdot T^{-1}$]	—	Mean flow rate
Q_a [$L^3 \cdot T^{-1}$]	—	Amplitude of the flow rate
r^2	—	Coefficient of determination
TDS [$M \cdot L^{-3}$]	—	Total dissolved solids
T_p [T]	—	Period of oscillation
$\bar{t}$ [T]	—	Real mean hydraulic retention time
t_t [T]	—	Theoretical mean hydraulic retention time
V [L^3]	—	Reactor volume

Greek

θ[–]	—	Dimensionless mean hydraulic retention time

Dimensionless parameters

$P_é$ [–]	—	Péclet number, $R_e P_r \propto \frac{mass\ transport\ by\ advection}{mass\ transport\ by\ diffusion}$
P_r [–]	—	Prandtl number, $\frac{viscous\ diffusion}{thermal\ diffusion}$
R_e [–]	—	Reynolds number, $\frac{inertial\ force}{viscous\ force}$
S_c [–]	—	Schmidt number, $\frac{viscous\ diffusion}{mass\ diffusion}$

References

[1] J. Makinia, S.A. Wells, Evaluation of empirical formulae for estimation of the longitudinal dispersion in activated sludge reactors, Water Res., 39 (2005) 1533–1542.
[2] B. De Clercq, F. Coen, B. Vanderhaegen, P.A. Vanrolleghem, Calibrating simple models for mixing and flow propagation in waste water treatment plants, Water Sci. Technol., 39 (4) (1999) 61–69.
[3] Y. Gao, F.J. Muzzio, M.G. Ierapetritou, A review of the residence time distribution (RTD) applications in solid unit operations, Powder Technol., 228 (2012) 416–423.
[4] D.C. de Freitas, F.H. Passig, C. Kreutz, K.Q. de Carvalho, E. J. Arantes, S.D. Gomes, Effect of hydraulic retention time on hydrodynamic behavior of anaerobic-aerobic fixed bed reactor treating cattle slaughterhouse effluent, Acta Sci. Techol., 39 (4) (2017) 469–476.
[5] O.N. Manjrekar, Y. Sun, L. He, Y.J. Tang, M.P. Dudukovic, Hydrodynamics and mass transfer coefficients in a bubble column photo-bioreactor, Chem. Eng. Sci., 168 (2017) 55–66.
[6] J.A. Jáuregui-Jáuregui, H.O. Méndez-Acosta, V. González-Álvarez, R. Snell-Castro, V. Alcaraz-González, J.J. Godon, Anaerobic treatment of tequila vinasses under seasonal operating conditions: Start-up, normal operation and restart-up after a long stop and starvation period, Bioresour. Technol., 168 (2014) 33–40.
[7] M. Mulas, S. Tronci, F. Corona, H. Haimi, P. Lindell, M. Heinonen, R. Vahala, R. Baratti, Predictive control of an activated sludge process: An application to the Viikinmäki wastewater treatment plant, J. Process Control, 35 (2015) 89–100.
[8] M. Rajasimman, S.V. Babu, N. Rajamohan, Biodegradation of textile dyeing industry wastewater using modified anaerobic sequential batch reactor – Start-up, parameter optimization and performance analysis, J. Tai. Inst. Chem. Eng., 72 (2017) 171–181.
[9] X. Tang, Y. Guo, B. Jiang, S. Liu, Metagenomic approaches to understanding bacterial communication during the anammox reactor start-up, Water Res., 136 (2018) 95–103.
[10] P.V. Danckwerts, Continuous flow systems. Distribution of residence times, Chem. Eng. Sci., 2 (1) (1953) 1–13.
[11] R.B. MacMullin, M. Weber, The theory of short-circuiting in continuous-flow mixing vessels in series and kinetics of chemical reactions in such systems. Trans. AIChE, 31 (2) (1935) 409–458.
[12] O. Levenspiel, Chemical reaction engineering, 3rd ed., Wiley & Sons Inc., New York, 1999.
[13] G.F. Froment, K.B. Bischoff, Non-steady state behavior of fixed bed catalytic reactors due to catalyst fouling, Chem. Eng. Sci., 16 (1961) 189–201.
[14] P.A.G. Encina, F. Fernández-Polanco, Behaviour of an anaerobic expanded bed reactor in non-steady state conditions, Wat. Res., 21 (11) (1987) 1329–1334.
[15] S. Claudel, J.P. Leclerc, L. Tétar, H.G. Lintz, A. Bernard, Recent extensions of the residence time distribution concept: unsteady state conditions and hydrodynamic model developments, Braz. J. Chem. Eng., 17 (4–7) (2000) 947–954.
[16] J.G. Boelhouwer, H.W. Piepers, A.A.H. Drinkenburg, Non-steady state operation of trickle-bed reactors, Stud. Surf. Sci. Catal., 133 (2001) 231–238.
[17] S. Yang, X. Li, Influences of extracellular polymeric substances (EPS) on the characteristics of activated sludge under non-steady-state conditions, Proc. Biochem., 44 (2009) 91–96.
[18] E.B. Nauman, Residence time distribution theory for unsteady stirred tank reactors, Chem. Eng. Sci., 24 (1969) 1461–1470.
[19] A. J. Niemi, Residence time distributions of variable flow process, Int. J. Ap. Rad. Iso., 28 (1977) 855–860.
[20] A.J. Niemi, Z. Kai, T. Jovan, M.J. Griffith, Tracer testing of processes under variable flow and volume, Nukleonika 43 (1) (1998) 73–94.
[21] J. Fernández-Sempere, R. Font-Montesinos, O. Espejo-Alcaraz, Residence time distribution for unsteady-state systems, Chem. Eng. Sci., 50 (1995) 223–230.
[22] L. Furman, J.P. Leclerc, Z. Stegowski, Tracer investigation of a packed column under variable flow. Chem. Eng. Sci., 60 (2005) 3043–3048.
[23] E. Domínguez, F. Ardila, S. Bustamante, System Solver: an open source tool for mathematically modelling dynamical systems, Ing. Inv., 30 (3) (2010) 157–164.

[24] Isee systems, Inc. 2018. STELLA: System Thinking for Education and Research. Availabe at: https://www.iseesystems.com/.
[25] The Math Works, Inc. 2018. SIMULINK: Simulation and Model Based Design. Available at: https://www.mathworks.com/products/simulink.html.
[26] Ventana Systems, Inc. 2018. Vensim industrial simulation software. Available at: http://vensim.com/.
[27] R.B. Chowdhury, G.A. Moore, A.J. Weatherley, M. Arora, A novel substance flow analysis model for analysing multi-year phosphorus flow at the regional scale, Sci. Total Environ., 572 (2016) 1269–1280.
[28] U.S. McKnight, S.G. Funder, J.J. Rasmussen, M. Finkel, P.J. Binning, P.L. Bjerg, An integrated model for assessing the risk of TCE groundwater contamination to human receptors and surface water ecosystems, Ecol. Eng., 36 (2010) 1126–1137.
[29] J.C.S.I. Gonçalves, M.F. Giorgetti, Mathematical model for the simulation of water quality in rivers using the Vensim PLE® software, J. Urb. Environ. Eng., 7 (1) (2013) 48–63.
[30] R. Chaves, D. López, F. Macías, J. Casares, C. Monterroso, Application of system dynamics technique to simulate the fate of persistent organic pollutants in soils, Chemosphere, 90 (2013) 2428–2434.
[31] H. Ibrahim, M. Pansu, D. Blavet, A. Hatira, P. McDonald, M. Bernoux, J. Drevon, Modelling the continuous exchange of carbon between living organisms, the soil and the atmosphere, Plant Soil, 398 (2016) 381–397.
[32] J. Álvarez, M. Roca, C. Valderrama, J.L. Cortina, A phosphorous flow analysis in spain, Sci. Total Environ., 612 (2018) 995–1006.
[33] F.R.A. Nascimento, A. Kiperstok, J. Martín, J. Morató, E. Cohim, Decision support system for management of reactive nitrogen flows in wastewater system, Environ. Sci. Pollut. Res., 25 (2018) 8644–8653.
[34] P. Fleury, V. Plagnes, M. Bakalowicz, Modelling of the functioning of karst aquifers with a reservoir model: Application to Fontaine de Vaucluse (South of France), J. Hydrol., 345 (2007) 38–49.
[35] A. Hartmann, M. Kralik, F. Humer, J. Lange, M. Weiler, Identification of a karst system's intrinsic hydrodynamic parameters: upscaling from single springs to the whole aquifer, Environ. Earth Sci., 65 (2012) 2377–2389.
[36] Y. Chang, J. Wu, G. Jiang, Modeling the hydrological behavior of a karst spring using a nonlinear reservoir-pipe model, Hidrog. J., 23 (2015) 901–914.
[37] G.M. von Medeazza, V. Moreau, Modelling of water–energy systems. The case of desalination, Energy, 32 (2007) 1024–1031.
[38] O. Sahin, R. Siems, R.G. Richards, F. Helfer, R.A. Stewart, Examining the potential for energy-positive bulk-water infrastructure to provide long-term urban water security: A systems approach, J. Clean. Prod., 143 (2017) 557–566.
[39] A. Ghasemi, B. Saghafian, S. Golian, System dynamics approach for simulating water resources of an urban water system with emphasis on sustainability of groundwater, Environ. Earth Sci., 76 (637) (2017) 1–15.
[40] R. Li, P. Guo, J. Li, Regional water use structure optimization under multiple uncertainties based on water resources vulnerability analysis, Water Resour. Manage., 32 (2018) 1827–1847.
[41] K. Kontomaris, T.J. Hanratty, Effect of molecular diffusivity on turbulent diffusion in isotropic turbulence, Int. J. Heat Mass Transfer, 36 (5) (1993) 1403–1412.
[42] O. Levenspiel, W.K. Smith, Notes on the diffusion-type model for the longitudinal mixing of fluids in flow, Chem. Eng. Sci., 50 (24) (1995) 3891–3896.
[43] M.F. Edwards, J.F. Richardson, Gas dispersion in packed beds, Chem. Eng. Sci., 23 (2) (1968) 109–123.
[44] Z. Dou, Z. Zhou, J. Wang, Y. Huang, Roughness scale dependence of the relationship between tracer longitudinal dispersion and Peclet number in variable-aperture fractures, Hydrol. Processes, 32 (2018) 1461–1475.
[45] D. Dochain, Analysis of the multiplicity of steady-state profiles of two tubular reactor models, Comput. Chem. Eng., 114 (2018) 318–324.
[46] V.V. Oliveira, M.V. Mateus, J.C.S.I. Gonçalves, A.G. Utsumi, M. F. Giorgetti, Prediction of the longitudinal dispersion coefficient for small watercourses, Acta Sci. Techol., 39 (3) (2017) 291–299.
[47] S.C. Chapra, R.P. Canale, Numerical methods for engineers, McGrawHill, 6th ed, 2008.
[48] Metcalf, Eddy, Wastewater engineering: treatment and reuse, McGrawHill, 4th ed, 2002.
[49] D.J.L. Costa, Mathematical model for hydrodynamic evaluation in non-steady state reactors. (in Portuguese). DSc. Thesis. EESC – USP, São Carlos, SP, Brazil, 2015. Available at: http://www.teses.usp.br/.
[50] M. Flury, T. Gimmi, Solute diffusion, in Methods of Soil Analysis, Part 4, Physical Methods, ed. by J.H. Dane, G.C. Topp, 1323–1351, SSSA, Madison, WI, 2002.
[51] R.B. Bird, W.E. Stewart, E.N. Lightfoot, Thermal conductivity and the mechanisms of energy transport. In: Transport Phenomena (Chapter 9), 2nd ed, 2002.
[52] E. Bianchi, G. Groppi, W. Schwieger, E. Tronconi, H. Freund, Numerical simulation of heat transfer in the near-wall region of tubular reactors packed with metal open-cell foams, Chem. Eng. J., 264 (2015) 268–279.
[53] N. Amini, Y.A. Hassan, Experimental study of bypass flow in near wall gaps of a pebble bed reactor using hot wire anemometry technique, Ann. Nuc. Ener., 65 (2014) 60–71.